Investigation of a triangular lattice photonic crystal patch antenna for terahertz communication systems

N. S. YOGA ANANTH[1,*], P. KARUPPASAMY[2]
[1]*Department of Electronics and Communication Engineering, P. S. R. Engineering College, Sivakasi, India*
[2]*Department of Electronics and Communication Engineering, Adithya Institute of Technology, Coimbatore, India*

A more efficient utilization of carrier frequencies to transmit data has recently emerged in the wireless bearer domain. The current research focuses on wireless communication with substantial data speeds and enhanced security. This article concentrates on designing a triangular lattice Photonic crystal (PhC) antenna structure and conducting subsequent research on its performance. The article offered a unique patch integrated with a diamond air holes PhC structure using the CST tool. The investigation of the proposed antenna is carried out using distinct sizes of diamond air holes and lattice constants of triangular PhC structure. In scenario 1, the diamond air hole in the triangular lattice PhC antenna design is varied between 2 and 6 μm in size to determine the optimal PhC antenna. Whereas, in scenario 2, the lattice value is varied from 13 to 23 μm. Based on the simulated results of two cases, the optimal PhC antenna produces the extreme results of -70.69 dB return loss (RL), 1.0058 voltage standing wave ratio (VSWR), and 8.74 dBi gain at 2.1 THz frequency. The proposed antenna frequency 2.1 THz is highly appropriate for future beyond 6G communication with enhanced data rate from giga to tera bits. The frequency band between 1-3 THz is optimal for various sensing and imaging applications. Especially 2.1 THz is great choice of non-destructive testing, hidden object detection since THz waves does not harm to humans.

(Received June 26, 2025; accepted February 4, 2026)

Keywords: Terahertz frequency, Patch antenna, Photonic crystals, Triangular lattice, Lattice constant

1. Introduction

Terahertz (THz) [1-4] technology is an emerging field in wireless communication [5-8] that connects microwave and optical frequencies. THz frequencies, which typically range from 0.1 to 10 THz, can handle extraordinarily high data rates [9-12]. The increase in frequency leads to a higher capacity for data transmission. The THz spectrum provides a significantly greater amount of bandwidth compared to a millimeter wave [13-15]. This surplus of bandwidth can facilitate high-speed wireless communication and also aid in reducing congestion. THz technology can facilitate highly detailed imaging and detection [16-18], which is advantageous for various outside communication applications, including airport security [19] and medical imaging [20,21]. THz communications exhibit greater directionality compared to microwave or millimeter wave communications due to reduced diffraction of free-space waves. THz experiences less signal attenuation than Infrared in some weather circumstances, such as fog. THz communication has the potential to serve as an alternative solution for addressing the challenges associated with last-mile and first-mile connectivity. These issues pertain to the creation of local [22], wide-area [23], multiple-user wireless connections for fast networks, such as those using fiber optics [24].

The unique features and wide range of uses of microstrip patch antennas [25-30] make them vital parts of contemporary communication systems. Patch antennas are renowned for their small and lightweight characteristics. Because of this, they are perfect for usage in portable and mobile products. Due to their compact dimensions, they can be seamlessly incorporated into gadgets without necessitating substantial space, a crucial aspect for preserving the streamlined appearance of today's electronic products. Although MPAs are extensively employed and provide numerous advantages, they are also subject to constraints regarding bandwidth, gain, efficiency, and material availability. To overcome these limitations, it is necessary to employ sophisticated design methodologies and meticulously choose appropriate materials and components. MPA's limitations can be addressed by utilizing techniques such as defective ground structure, metamaterials, and PhC. This paper utilizes the PhC technique to address the constraints of patch antennas and improve their performance.

2. Photonic crystal structure and design

PhC [31-34] is an organic structure whose refractive index varies regularly. PhC features orthogonally bored low-dielectric constant air holes, known as PBG, into high-dielectric material to completely prevent electromagnetic wave transmission, allowing for frequency selection in both directions. PhC's refractive index varies periodically, usually on the light wavelength scale. The triangular pattern of dielectric rods or holes causes this periodicity in a triangular lattice PhC. The interference creates a photonic bandgap (PBG) [35-36] that "forbids" specific EM frequencies from passing through the crystal. This bandgap

effectively disperses or reduces EM waves in the crystal by prohibiting their propagation in either direction.

In PhC, the choice of lattice structure influences the PBG qualities, EM wave propagation features, and overall efficiency of the PhC. Figures 1 (a) and (b) illustrate the two lattice structures found in 2D PhC: triangle and square.

Patch antenna performance can be greatly improved by incorporating a triangular lattice [37-40] PhC into the design. This allows for innovative manipulation of electromagnetic waves. PhC structures can lead to improvements in radiation efficiency, bandwidth, and even antenna structure miniaturization. Surface waves [41-43] have the potential to produce counterfeit radiation and decrease the radiation efficiency of a patch antenna. Surface waves are undesired electromagnetic waves that travel along the substrate's surface. The triangular lattice PhC produces a PBG that can suppress these surface waves, resulting in a more effective antenna with minimal sidelobes. The addition of a triangular lattice PhC can alter the effective permittivity of the patch antenna substrate, resulting in a wider bandwidth. This is particularly advantageous for contemporary communication networks that need antennas to function across a large frequency spectrum. Because of its distinct dispersion characteristics, the PhC structure reduces the effective wavelength of electromagnetic waves. This allows for the construction of smaller antennas without compromising functionality, allowing them to be integrated into condensed gadgets such as IoT and smartphone devices. By varying the lattice constant and the hole sizes in the triangular lattice PhC, one can tune the PBG to particular frequency ranges. This allows designers the freedom to optimize the antenna for specific applications.

The existing PhC research works are discussed as, Kumar et al. [44] investigated the performances of patch antenna with a triangular lattice PhC structure background. In the PhC substrate, the air hole is designed with inner and outer hole radii antenna and the antenna is resonated at 11.10 THz. This antenna is applicable for various applications such as satellites, 5G wireless networks, aerospace, and aircraft register. Pandian et al. [45] proposed a patch antenna that utilizes a square lattice PhC structure. The authors proposed a unique patch antenna and optimized the structure using four different scenarios. The proposed antenna worked at 1.5 THz and the outcomes are -33.7 dB RL, 1.022 VSWR and 286 GHz bandwidth. The PhC reveals the antenna frequency and specificity, which are significant in the microwave field. The stopband rejects most of the intensity radiated by an antenna mounted on the PhC's layer, without reducing the driving-point impedance.

Kumar et al. [46] introduced the PhC antenna and examined its efficacy by adjusting the air gap radius. The proposed antenna is also capable of operating within the multi-frequency terahertz spectrum. Using a photonic band gap (PBG) on a crystal substrate increases the RL from -29 to -44 dB. The bandwidth of the antenna array was further enhanced from 40 to 110 GHz. Kumar et al. [47] designed a rectangular MPA integrated with PhC structure and the structure is simulated using the HFSS tool. The analysis outlines the process of optimizing the radius of cylindrical perforations, leading to alterations in various antenna characteristics as the hole radius changes. The lowest RL of −33.69 dB is observed at 28.3 GHz, with a bandwidth of 1.30 GHz and a gain of 3.13 dB.

Britto et al. [48] investigated the PhC antenna performances with a slotted patch model. This feature improves the VSWR to 1.002 at 2.37 THz operating frequencies, as well as the RL to -57.81 dB. Applications that require higher data rate transmission benefit from an increase in hole radius because it causes the zero-dispersion point to shift towards a shorter wavelength. Temmar et al. [49] proposed and evaluated a terahertz microstrip patch antenna around 0.65 GHz, the frequency at which various terahertz communication and sensing applications are popular. The antenna is based on an altered silicon-air PBG substrate. The proposed antenna is constructed on a PhC substrate that is being examined to improve the antenna's characteristics at 0.65 THz by reducing the presence of undesirable surface waves.

The majority of the works are based on square lattice [50-54] PhC antennae, as indicated by the research survey. Only a handful of works have addressed the triangular lattice PhC structure, identifying a lacuna. All current research has implemented cylindrical air openings in the PhC lattice structure. Therefore, this research article proposes a plausible model of a diamond air hole in a triangular lattice structure and investigates the characteristics of the PhC antenna. The diamond air holes promote anisotropic perturbations in the dielectric circulation, which augments control over the propagation features of surface and leaky modes. This configuration improves electromagnetic field constriction due to short angles that enhance local electric field magnitude, therefore enhancement of radiation efficiency and bandwidth. Beyond that, the suggested antenna produces a very high data rate, resonates at 2.1 THz, and is completely safe for human use.

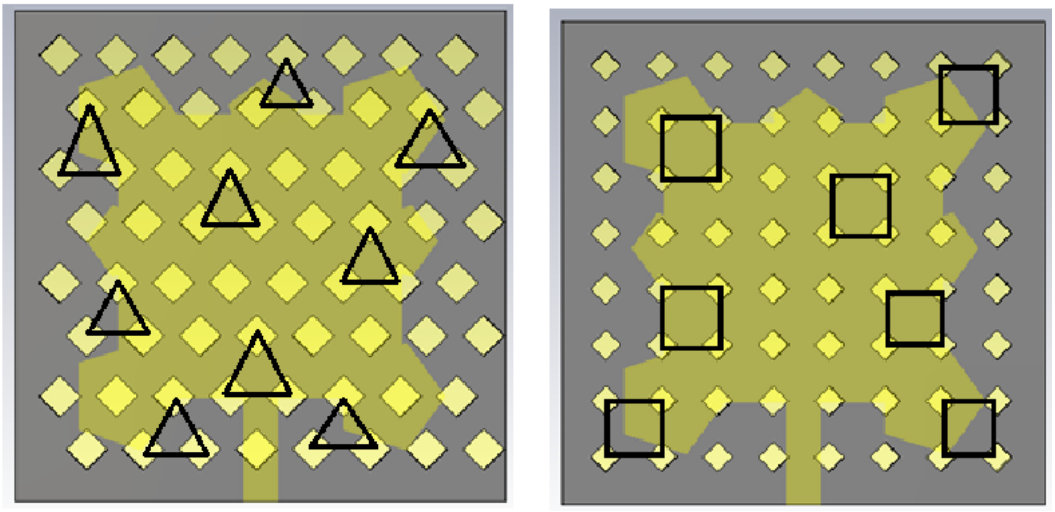

(a) (b)

Fig. 1. PhC structure: (a) Triangular lattice, (b) Square lattice (colour online)

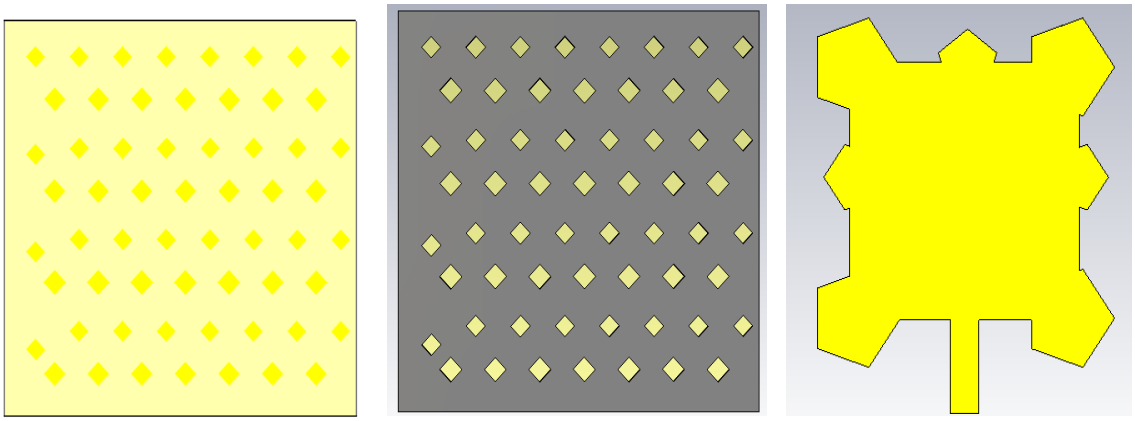

(a) (b) (c)

Fig. 2. (a) Ground, (b) PhC Substrate, (c) Patch (colour online)

Table 1. Parametric study of various sizes of diamond holes in PhC structure

Diamond hole size (µm)	Frequency (THz)	RL (dB)	VSWR	Gain (dBi)	Directivity (dB)	Bandwidth (THz)
2	2.174	-34.37	1.0389	7.791	8.230	0.387
2.5	2.020	-36.50	1.0379	7.820	8.345	0.382
3	2.114	-52.92	1.0056	8.381	8.812	0.398
3.5	2.114	-55.60	1.0033	8.421	8.824	0.403
4	2.113	-58.30	1.0024	8.530	8.902	0.410
4.5	2.111	-63.67	1.0013	8.701	8.952	0.452
5	2.110	-70.69	1.0058	8.748	8.962	0.467
5.5	2.108	-61.95	1.0015	8.592	8.911	0.435
6	2.020	-32.67	1.0361	7.892	8.119	0.377

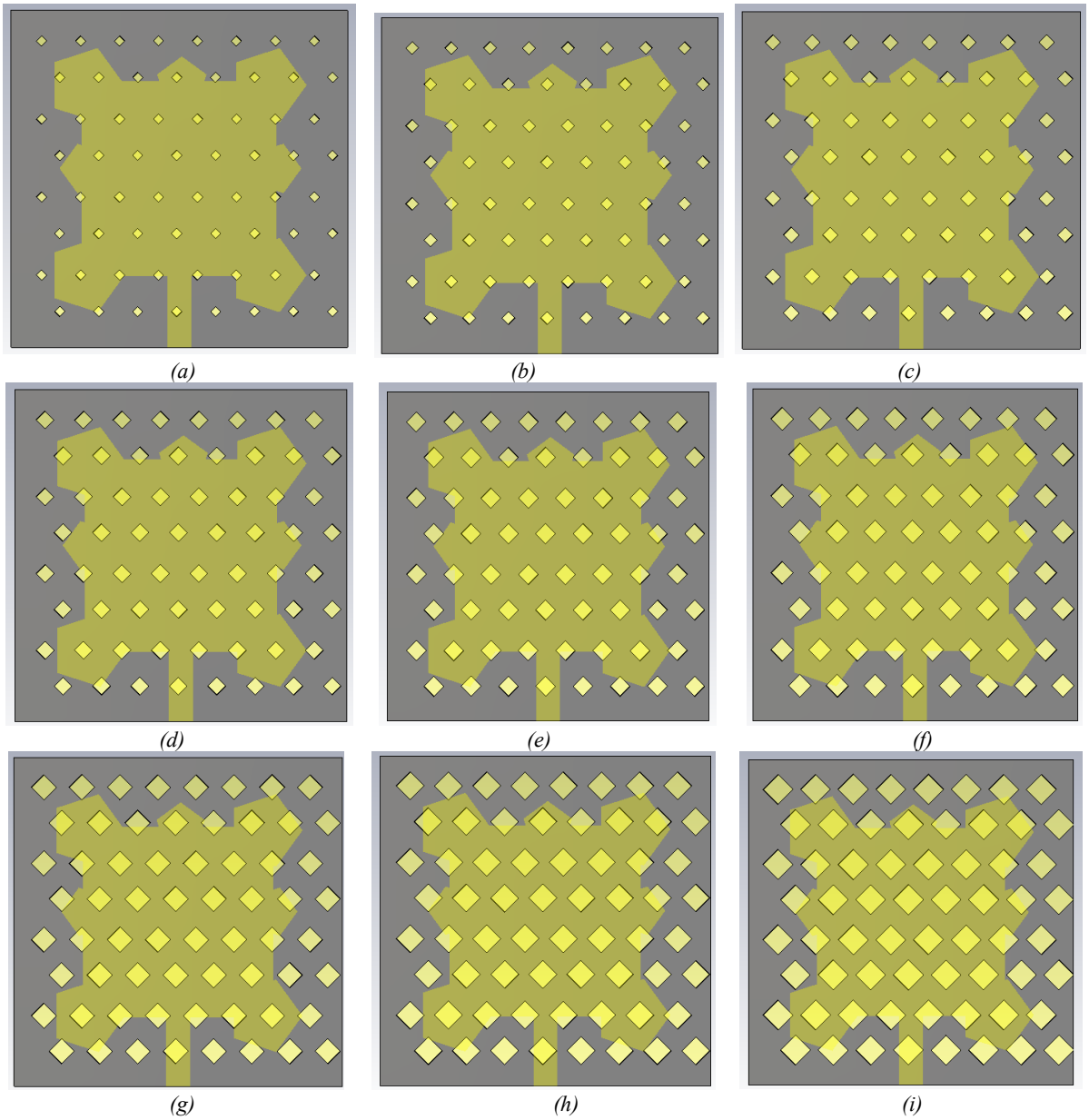

Fig. 3. Diamond air holes in triangular lattice PhC structure: (a) 2 µm, (b) 2.5 µm, (c) 3 µm, (d) 3.5 µm, (e) 4 µm, (f) 4.5 µm, (g) 5 µm, (h) 5.5 µm, (i) 6 µm (colour online)

3. Steps to design a triangular PhC Patch antenna structure

The design of a triangular lattice PhC patch antenna [55] entails several steps, including the following:

The proposed patch antenna design involves three distinct layers of ground (150x150 µm^2), substrate (150x150 µm^2), and patch (90x90 µm^2) with feed (32x9.6 µm^2).

The patch width and length are calculated as,

$$P_W = \frac{c_0}{2f_{res}}\sqrt{\frac{2}{\varepsilon_r + 1}} \tag{1}$$

$$P_L = \frac{c_0}{2f_{res}\sqrt{\varepsilon_{reff}}} - 2\Delta L \tag{2}$$

Design the ground layer with copper material, as shown in Fig. 2(a).

$$G_L = S_L = 6 * h + P_L \tag{3}$$

$$G_W = S_W = 6 * h + P_w \tag{4}$$

Design the conventional substrate layer using Roger R5880 material. It is highly preferred in THz antenna, low lass tangent, reduce signal attenuation, enhance radiation efficient. Rogers substrates deliver high precision, low loss,

and superior reliability, making them ideal for high-frequency, mm-wave, and THz antenna applications compared to other conventional substrates.

To design a PhC substrate, air hole and lattice shapes are to be selected. The design prefers a diamond air hole and a triangular lattice structure based on the requirements.

Fig. 2 (c) illustrates how to punch the diamond-shaped air holes equidistant to create the triangular lattice PhC structure.

Design the patch layer with the distinct shape of a square patch incorporated with a pentagon pentagon-cornered structure. Fig. 2(c) illustrates the distinct patch element.

4. Impact of various sizes of diamond air holes in triangular lattice PhC

This section simulates the design of a triangular lattice PhC antenna and investigates its performances. By incorporating a hole-type pattern in a triangular lattice structure, the PhC substrate replaces the conventional patch antenna substrate. This article opts for a unique diamond air hole rather than a regular cylindrical airhole shape. The triangular lattice pattern, which distinguishes between odd and even rows, results in non-identical rows. In both odd and even air, the geometry of diamond air holes is the same. Hence, the diamond air holes are drilled into the substrate layer with even and odd row patterns.

To evaluate the PhC antenna characteristics, the diamond air hole in the triangular lattice is optimized for different sizes from 2μm to 6μm with a step size of 0.5μm. Hence, the structure of triangular PhC is designed for various diamond air hole sizes, as illustrated in figure 3 (a-i). The CST tool simulates the designed PhC structure, and Table I highlights the output parameters. As the size of the air hole increases gradually, so do the antenna's performances, which decrease as the air hole size increases. It is observed that the antenna produces better performances at mid-range of air hole size. The PhC antenna works very well, with -70.69 dB RL, 1.00584 VSWR, and 8.762 dB directivity at 2.11 THz. Its best feature is the triangular PhC lattice structure with the diamond air hole at 5 μm. Fig. 4 illustrates the RL performances of various diamond hole size PhC structures. The RL is -30 dB for diamond air holes that are 2, 2.5, and 6 μm in size, -50 dB for structures that are 3, 3.5, and 4 μm in size, and over 60 dB for PhC structures with air holes that are 4.5, 5, and 5.5 μm in size. Fig. 5 (a) and (b) show the gain and directivity comparison of various triangular lattice PhC structures. The gain and directivity demonstrate an extensive enhancement as the diamond hole magnitude intensifies from 2 to 5 μm, representing amended electromagnetic confinement and reduced the surface-wave over this range. The antenna achieves superlative radiation metrics at roughly 5 μm, where the dielectric contrast and photonic bandgap interaction are most efficiently harmonized. Nonetheless, enlarging the hole magnitude further outcomes in a swift weakening of both characteristics, as the increased air fraction disturbs the field distribution and moderates the resonant behavior.

5. Consequences of distinct lattice values of triangular lattice PhC structure

The lattice constant is a critical parameter in PhC design because it directly influences the crystal's capacity to manipulate EM waves in the structure. The distance between repeating cylindrical air holes or rods, arranged in a 2D pattern (like a square or triangular lattice), is known as the lattice constant in 2D PhCs. The lattice constant for 2D PhCs is usually between a few hundred nm and μm. So, this part looks at the triangular PhC structure for different lattice values between 13 μm and 21 μm, with diamond-shaped air holes in the triangular lattice structures. Fig. 6 (a-e) illustrates the design of five distinct PhC antennas for varying lattice constant values.

Table 2 highlights the outcomes of the simulation of the designed PhC structures. Fig. 7 displays the RL observations in three different ranges: 50 dB, 60 dB, and 70 dB. When the lattice constant is 15 μm, the PhC structure produces the extreme result of -70.69 dB RL at 2.11 THz. When the lattice value of 15 μm, the PhC periodicity is aligned well and effective the operating frequency of 2.1 THz which allows strong suppression of EM waves. This enhanced bandgap interaction leads to increase the impedance matching among the patch and its surroundings.

Fig. 8 (a) and (b) illustrate the investigation of gain and directivity. The cautious regulation of the lattice constant allows for designing PhCs with specific optical properties for various photonic and optoelectronic applications. The optimization of lattice constant strengthens the periodicity's configuration with the operating wavelength, which in turn reinforces the clampdown of surface waves and the vertical radiation, foremost to augmented gain and directivity.

6. Comparison of proposed work with existing PhC works

Table 3 lists the analysis that compares the proposed PhC works with current PhC-related antennas. In this instance, four antenna works produced the lowest RL, approximately 50 dB; five other antennas produced RL in the vicinity of 40 dB; whereas the proposed PhC antenna produced RL of 70 dB. Compared to previous efforts, the suggested antenna's VSWR is significantly lower (1.00584). Furthermore, the proposed work's bandwidth is superior to that of other antennas. The suggested antenna result is outstanding since the research centers on the triangular lattice PhC structure. An antenna's radiation pattern is determined by its E and H fields. It is a graphical representation of the radiated field's relative magnitude in different directions from the antenna. Fig. 9 (a) and (b) illustrate the E and H field monitors of the optimized triangular PhC structure.

An antenna's radiation pattern is determined by its E and H fields. It is a graphical representation of the radiated field's relative magnitude in different directions from the

antenna. Fig. 9 (a) and (b) illustrate the E and H field monitors of the optimized triangular PhC structure. The E-field distribution in Fig. 9(a) shows strong confinement across the patch surface and enhanced field intensity near the diamond-shaped holes, indicating effective dielectric perturbation and suppression of surface-wave leakage by the PhC lattice. The smooth field transition across the structure confirms efficient coupling between the feed and the resonant mode. In Fig. 9(b), the H-field pattern displays well-formed magnetic loops along the patch edges and around the photonic crystal boundaries, signifying stable resonance and efficient energy circulation. Fig. 10 (a) and (b) illustrates the polar and 3D plot of the radiation characteristics of the optimized PhC antenna structure. The electromagnetic waves that emanate from the antenna are orthogonal to one another and change with time and space.

The ultra-tiny details dimensions are needed for THz antenna fabrication are frequently too trivial for traditional lithography practices to handle, assembly the process very problematic. Material losses, surface roughness, and metal conductivity restrictions take center stage at these dimensions, sternly reducing antenna characteristics even for relatively small fabrication flaws. It is also challenging to put into practice because research into appropriate low-loss materials and accurate etching procedures for THz devices is ongoing. Since the practicality of fabrication is currently limited by current micro-/nanofabrication technologies, most studies on THz antennas rely on simulations.

Table 2. Parametric study of various lattice values of PhC structure

PhC lattice values (µm)	Frequency (THz)	RL (dB)	VSWR	Gain (dBi)	Directivity (dB)	Bandwidth (THz)
L=13	2.111	-64.89	1.0011	8.031	8.431	0.413
L=15	2.110	-70.69	1.0058	8.748	8.962	0.467
L=17	2.113	-56.29	1.0030	8.520	8.691	0.449
L=19	2.113	-56.79	1.0028	7.916	8.201	0.413
L=21	2.113	-55.82	1.0032	7.720	7.920	0.395
L=23	2.113	-54.62	1.0037	7.419	7.821	0.382

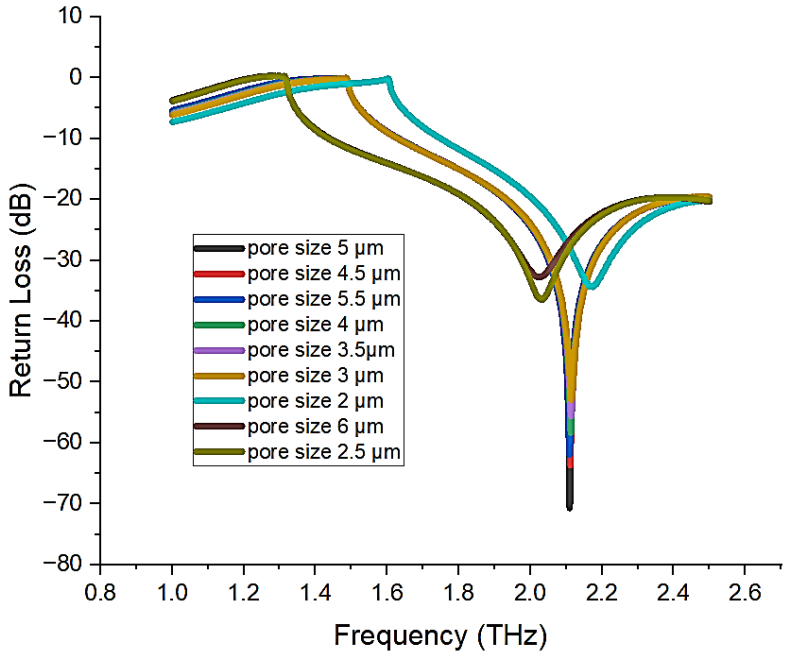

Fig. 4. RL performance of various hole sizes in PhC structure (colour online)

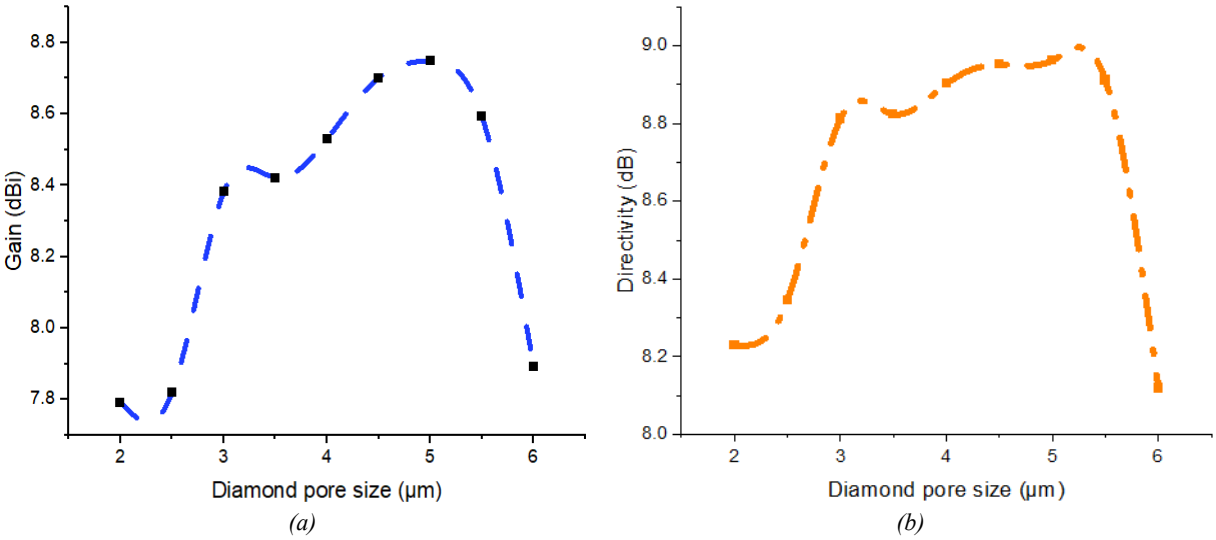

Fig. 5. (a) Gain vs diamond air hole size, (b) Directivity vs diamond air hole size (colour online)

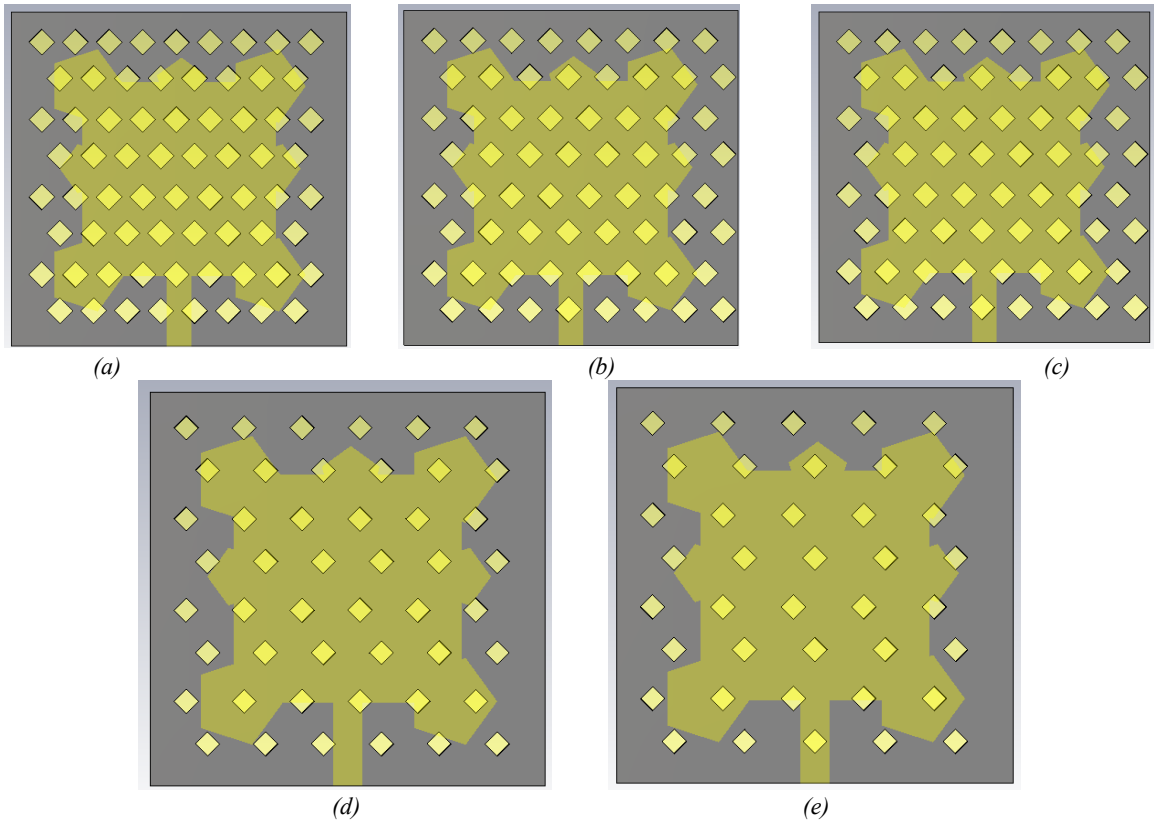

Fig. 6. PhC antenna for distinct lattice constant: (a) a =13 μm, (b) b =15 μm, (c) c =17 μm, (d) d =19 μm, (e) a =21 μm (colour online)

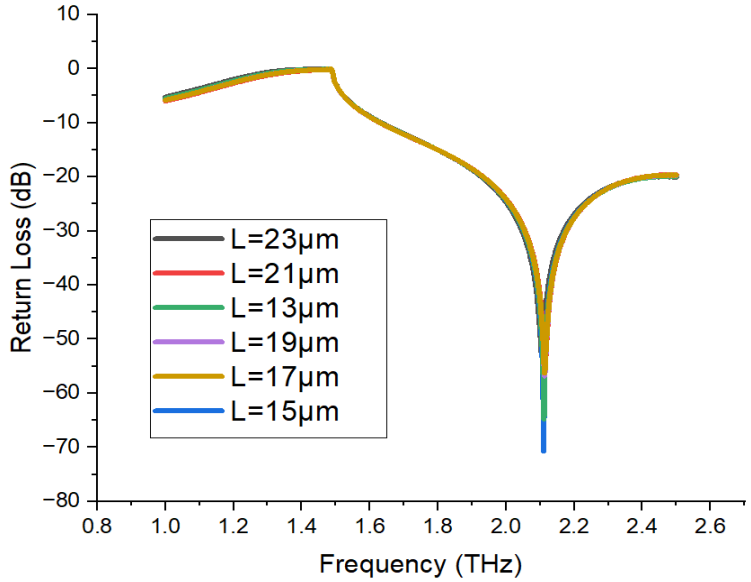

Fig. 7. RL comparison of various lattice values (colour online)

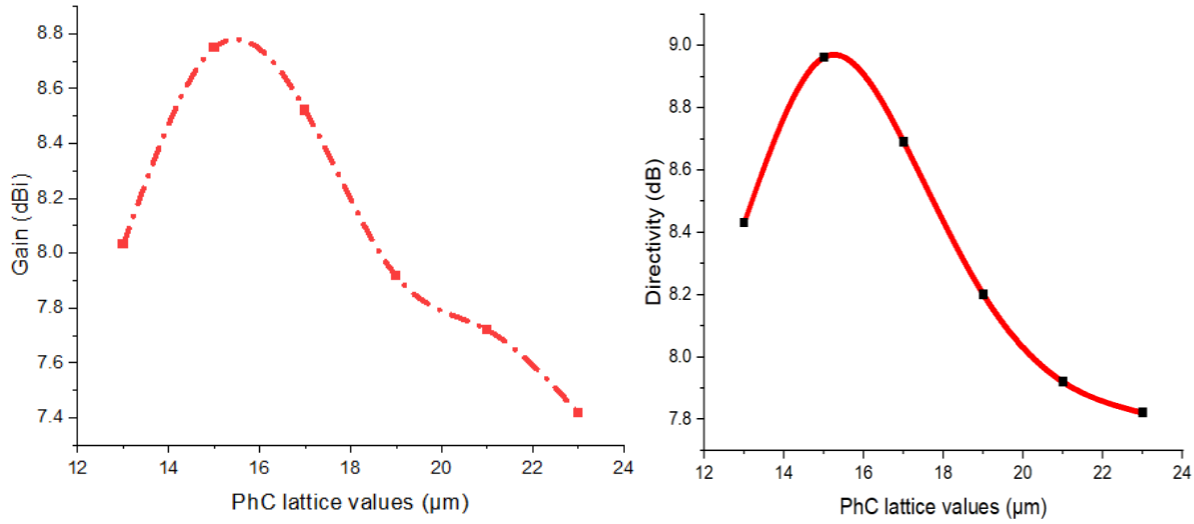

(a) *(b)*

Fig. 8. (a) Gain vs lattice values, (b) Directivity vs lattice values (colour online)

Table 3. It lists the analysis that compares the proposed PhC works with current PhC (colour online)

Parameters	Proposed antenna	Britto et al. [2020]	Kumar et al. [2020]	Khezzar et al. [2021]	Aloui et al. [2022]	Bai and Li [2023]	Li et al. [2024]	Pandian et al. [2024]	A.Youssef et al. [2024]	Danasegaran et al. [2024]
Freq. (THz)	2.11	2.37	11.10	0.3	4.15	1.267	0.692	1.55	1.13	1.59
RL (dB)	-70.69	-57.81	-41.82	-58.70	-32.5	-58.11	-64.1	-33.78	-41.81	-31
VSWR	1.00584	1.002	1.01	-	1.25	-	-	1.022	1.080	1.052
Gain (dBi)	8.748		1.14	9.43	7.5	3.173	7.66	-	9.4	--
Dir (dB)	8.962	7.68	1.93	133 G	-			-	-	2.83
BW	0.467 THz	0.052 THz	-	-	-	-	-	286 GHz	110 GHz	-

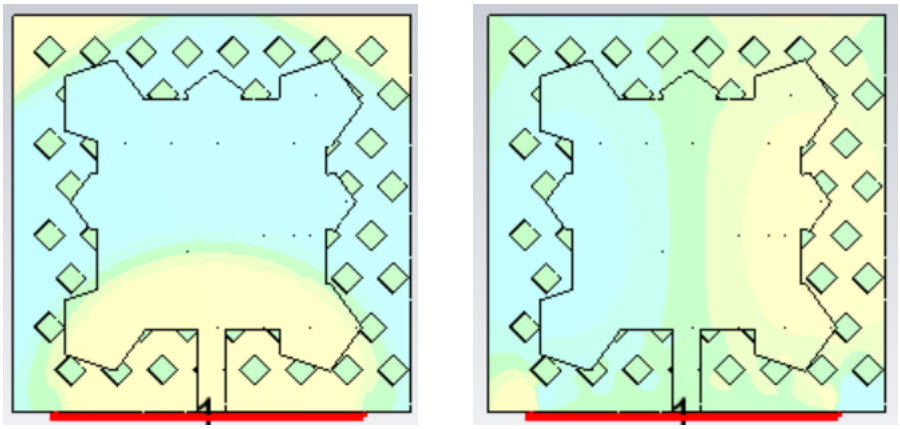

(a) (b)

Fig. 9. (a) E field, (b) H field monitor of optimized PhC structure (colour online)

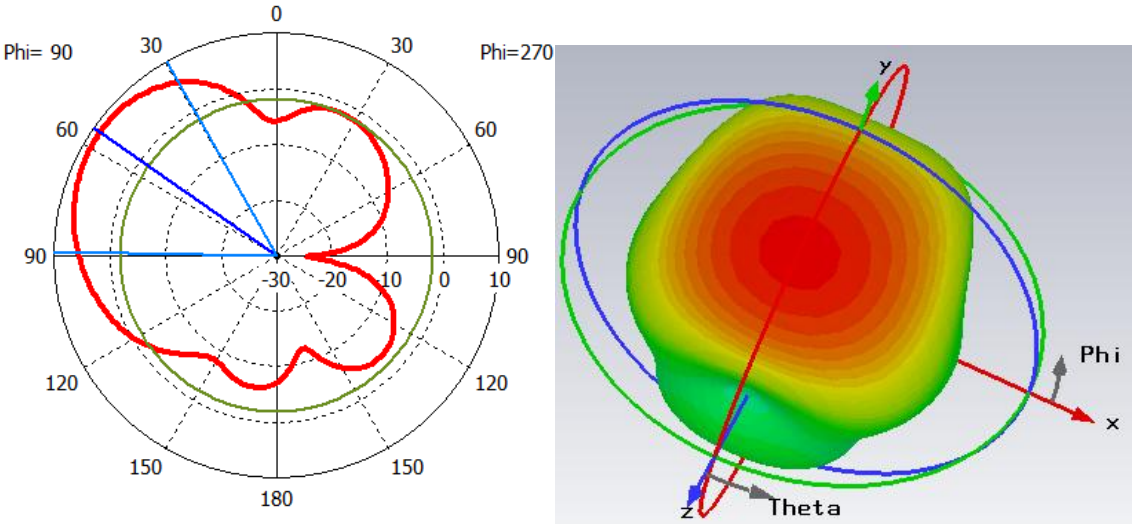

(a) (b)

Fig. 10. Radiation characteristics: (a) polar plot, (b) 3D curve (colour online)

7. Conclusion

This article illustrates that the PhC antenna has a substantial impact on potent electromagnetic radiation and will be a significant factor in the development of contemporary wireless devices. The study also explores the propagation of electromagnetic waves in a triangular PhC substrate as a function of diamond hole size and lattice constant.

With their periodic structure, PhC enable improved radiation pattern control, which may lead to a decrease in backscatter and sidelobes. It tends to improve the overall antenna performance. As a result, the small footprint of the proposed PhC antenna is highly beneficial for wireless communications, as it delivers a significantly higher Tbps data rate and facilitates a wide range of applications in the THz frequency.

References

[1] M. Alibakhshikenari, B. S. Virdee, S. Salekzamankhani, S. Aissa, C. H. See, N. Soin, S. J. Fishlock, A. A. Althuwayb, R. Abd-Alhameed, I. Huynen, James A McLaughlin, Francisco Falcone, Ernesto Limiti, Sci. Rep. **11**, 10218 (2021).

[2] X. Ji, Y. Chen, J. Li, D. Wang, Y. Zhao, Q. Wu, M. Li, Micromachines **15**(3), 407 (2024).

[3] Terahertz radiation, Wikipedia. https://en.wikipedia.org/wiki/Terahertz_radiation, 2024.

[4] H. Elayan, O. Amin, B. Shihada, R. M. Shubair, M.-S. Alouini, IEEE Open Journal of the Communications Society **1**, 1 (2020).

[5] A. Boufrioua, Wireless Personal Communications **110**(4), 1879 (2020).

[6] J. Raghunath, P. Kumar, T. Ali, P. Kumar, S. D. Ghouse, S. Pathan, Journal of Sensor and Actuator Network **12**(5), 69 (2023).

[7] S. P. J. Christydass, N. Gunavathi, Progress in Electromagnetics Research C **113**, 97 (2021).

[8] A. Hirata, M. Yaita, IEEE Trans. THz Sci. Technol. **5**(6), 1128 (2015).

[9] H. Yang, S.-Y. Xu, G.-P. Jiang, IEEE Transactions on Circuits and Systems II: Express Briefs **68**(4), 1487 (2021).
[10] H. Yan, G. Chang, Z. Ma, L. Lin, IEEE Communications Letters **22**(9), 1782 (2018).
[11] F. Strömbeck, H. Zirath, Asia-Pacific Microwave Conference (APMC), Yokohama, Japan, 55, 2022.
[12] M. P. V. Sahul, Ankit Agarwal, S. Somasundaram, Gaurav Upadhyay, K. Thenmozhi Selvi, P. S. Sura, Subramanya Udupa, 4th International Conference on Power, Control & Embedded Systems (ICPCES), Allahabad, India, 1, 2017.
[13] B. Yang, H. J. Qian, J. Zhou, Y. Shu, X. Luo, IEEE Journal of Solid-State Circuits **58**(3), 691 (2023).
[14] M. Naftaly, A. P. Flouds, A. G. Davies, Int. J. Infrared Millimeter Waves **26**, 55 (2005)
[15] T. Robin, C. Bouye, J. Cochard, Proc. SPIE **8985**, Terahertz, RF, Millimeter, and Submillimeter-Wave Technology and Applications VII, 898512 (2014).
[16] S. Azizi, S. Nouri-Novin, M. M. Seyedsharbaty, F. B. Zarrabi, Optical and Quantum Electronics **50**(6), 230 (2018).
[17] E. C. Britto, S. K. Danasegaran, K. Sagadevan, Metamaterial Technology and Intelligent Metasurfaces for Wireless Communication Systems, S. Mehta, A. Abougreen (eds.), IGI Global, Pennsylvania, 180 (2023).
[18] M. Esfandiyari, A. Lalbakhsh, S. Jarchi, M. Ghaffari-Miab, H. N. Mahtaj, R. B. V. B. Simorangkir, Materials and Design **220**, 110855 (2022).
[19] Amelia Carr, Tania Biswas, Jane V. Wheeler, Journal of Air Transport Management **85**, 101814 (2020).
[20] Md. T. Islam, M. T. Islam, M. Samsuzzaman, H. Arshad, H. Rmili, IEEE Access **8**, 227678 (2020).
[21] G. Rajalakshmi, Sathish Kumar Danasegaran, R. Pandian, N. Jaypal, S. Lalithakumari, Optical and Quantum Electronics **56**, 1282 (2024).
[22] H. M. El-Hageen, Y. H. Alfaifi, H. Albalawi, Ahmed Alzahmi, Aadel M. Alatwi, Ahmed F. Ali, Mohamed A. Mead, Journal of Network and Systems Management **32**, 85 (2024).
[23] A. Agarwal, G. Misra, K. Agarwal, Am. J. Electr. Electron. Eng. **3**(2), 22 (2015).
[24] S. N. Khonina, N. L. Kazanskiy, M. A. Butt, Biosensors **13**(9), 835 (2023).
[25] D. S. Kumar, S. Pavithra, K. S. Ranjith, R. Kiruthika, E. Kavin, 7th International Conference on Electronics, Communication and Aerospace Technology (ICECA), Coimbatore, India, 1464, 2023.
[26] A. S. Alqahtani, Opt. Quant. Electron. **55**, 1014 (2023).
[27] Ali Ameri, Gholamreza Moradi, Reza Sarraf Shirazi, Optics Continuum **2**(5), 1148 (2023).
[28] M. N. E. Temmar, A. Hocini, D. Khedrouche, M. Zamani, J. Comput. Electron. **18**, 231 (2019).
[29] A. Hocini, M. N. Temmar, D. Khedrouche, M. Zamani, Photonics Nanostruct. Fundam. Appl. **36**, 100723 (2019).
[30] R. K. Kushwaha, P. Karuppanan, Optik **200**, 163422 (2020).
[31] A. Nejati, F. B. Zarrabi, M. Rahimi, Zahra Mansouri, Optik **126**(19), 2153 (2015).
[32] M. Shalini, M. Ganesh Madhan, Photonics and Nanostructures - Fundamentals and Applications **51**, 101046 (2022).
[33] S. K. Danasegaran, E. C. Britto, S. Dhanasekaran, G. Rajalakshmi, S. Lalithakumari, A. Sivasangari, G. Sathish Kumar, (2024). Radar and RF Front End System Designs for Wireless Systems, S. Mehta and Rupesh Kumar (Eds.), IGI Global, 176 (2024).
[34] Inzamam Ahmad, Sadiq Ullah, Shakir Ullah, Usman Habib, Sarosh Ahmad, Adnan Ghaffar, Mohammad Alibakhshikenari, Salahuddin Khan, Ernesto Limiti, Electronics **10**(16), 1941 (2021).
[35] S. Thakur, N. Singh, Optik **242**, 167355 (2021).
[36] Xiyuan Lu, Ashish Chanana, Yi Sun, Andrew McClung, Marcelo Davanco, Kartik Srinivasan, Optics Express **32**, 06594 (2024).
[37] Francis Segovia-Chaves, Herbert Vinck-Posada, Optik **181**, 1013 (2019).
[38] Haroldo Hattori, Christian Seassal, Xavier Letartre, Pedro Rojo-Romeo, Jean-Louis Leclercq, P. Viktorovitch, M. Zussy, Léa Cioccio, Loubna Melhaoui, Jean-Marc Fedeli, Optics Express **13**(9), 3310 (2005).
[39] Guoyan Dong, Ji Zhou, Xiulun Yang, Xiang Meng, Progress in Electromagnetics Research **128**, 91 (2012).
[40] Zetao Ma, Kazuhiko Ogusu, Optics Communications **282**(7), 1322 (2009).
[41] K. Mahendran, Sathish Kumar Danasegaran, R. Indhu, S. Annie Angeline Preethi, J. Optoelectron. Adv. M. **26**(3-4), 106 (2024).
[42] M. Popov, Journal of Mathematical Sciences **283**, 641 (2024).
[43] S. Lalithakumari, S. K. Danasegaran, G. Rajalakshmi, R. Pandian, E. C. Britto, Brazilian Journal of Physics **53**, 140 (2023).
[44] D. S. Kumar, B. E. Caroline, S. Thilagavathi, International Conference on System, Computation, Automation and Networking (ICSCAN), Pondicherry, India, 1, 2020.
[45] R. Pandian, S. K. Danasegaran, S. Lalithakumari, G. Rajalakshmi, G. Sathish Kumar, Optical and Quantum Electronics **56**, 763 (2024).
[46] C. Kumar, S. K. Raghuwanshi, V. Kumar, Journal of Electromagnetic Waves and Applications **38**(2), 250 (2024).
[47] C. Kumar, S. K. Raghuwanshi, V. Kumar, Front. Mater. **9**, 1079588 (2022).
[48] Elizabeth Caroline Britto, Sathish Kumar Danasegaran, William Johnson, International Journal of Communication Systems **34**(1), e 4662 (2020).
[49] Mohamed Nasr Eddine Temmar, Abdesselam Hocini, Djamel Khedrouche, Tayeb Ahmed Denidni, Optik **217**, 164897 (2020).

[50] Sathish Kumar Danasegaran, Elizabeth Caroli Britto, K. Sagadevan, M. Paranthaman, S. Poonguzhali, Mahendran Krishnakumar, Brazilian Journal of Physics **54**(1), 31 (2024).
[51] G. Li, C. Huang, R. Huang, B. Tang, J. Huang, J. Tan, N. Xia, H. Cui, Photonics **11**(4), 307 (2024).
[52] Amraoui Youssef, Imane Halkhams, Rachid El Alami, Mohammed Ouazzani Jamil, Hassan Qjidaa, Results in Engineering **22**, 102327 (2024).
[53] Y. Bai, J. Li, Optoelectron. Lett. **19**, 666 (2023).
[54] D. Khezzar, D. Khedrouche, T. A. Denidni, Photonics and Nanostructures - Fundamentals and Applications **46**, 100947 (2021).
[55] C. A. Balanic, Antenna theory: analysis and design, Hoboken (NJ): John Wiley & Sons Inc., 1997.
[56] K. Mahendran, H. Sudarsan, S. Rathika, AEU – International Journal of Electronics and Communications **161**, 154543 (2023).
[57] K. Mahendran, Sathish Kumar danasegaran, R. Indhu, S. Annie Angeline Preethi, J. Optoelectron. Adv. M. **26**(3-4), 106 (2024).

*Corresponding author: yogaananthnspsr@gmail.com